A NEW APPROACH TO CONTROL SINGLE-LINK FLEXIBLE ARMS. PART I: Modelling and Identification in the Presence of Joint Friction

Vicente Feliu[1], Kuldip S. Rattan[2] and H. Benjamin Brown, Jr.

CMU-RI-TR-89-8

The Robotics Institute
Carnegie Mellon University
Pittsburgh, Pennsylvania 15213

March 1989

---

[1]Visiting Professor, Dpto Ingeniería Eléctrica, Electrónica y Control, UNED, Ciudad Universitaria, Madrid-28040, Spain

[2]Visiting Professor, Department of Electrical Systems Engineering, Wright State University, Dayton, OH. 45435.

Table of Contents

List of Figures

Abstract

This report presents a new way to model and identify single-link flexible arms when Coulomb friction is present in the joint. In order to isolate the effects of this nonlinearity, the arm model is divided into two submodels: motor and beam. The two are coupled through the torque at the base of the beam.

A systematic method is developed to obtain the dynamics of a lumped-mass flexible beam, and some properties are obtained from this model. The influence of the payload on the model is given special attention. This way of modelling is later extended to the general case of distributed-mass flexible arms.

Identification in the presence of Coulomb friction is carried out. A new method is proposed to estimate this friction and to reconstruct the motor frequency response from experimental results, which are highly distorted by this nonlinear friction.

Experimental results are presented and, finally, conclusions are drawn.

1. Introduction

1.1. General Introduction

An important research effort has been carried out in the past few years to study the control of flexible structures and, in particular, flexible arms. Several papers have appeared on this topic studying different aspects: [1,2] are examples of controlling the endpoint position using state space techniques; [3-5] used different schemes of adaptive controllers in order to take into account changes in the load. Classical frequency domain techniques to control a flexible arm with two degrees of freedom were used in [6]. However, very little effort has been devoted to the control of flexible arms when static and dynamic frictions are present in the joints, even though this case is very common in practice.

Our work is devoted to solving or at least minimizing problems due to nonlinear friction, which may be very noticeable in lightweight flexible arms, or in flexible arms moving at low speeds and accelerations. We propose a completely new way of modelling, identifying and controlling these arms that produces simpler controllers than the other methods. Our final goal is to build and control a 3-joint flexible arm with 3 degrees of freedom, but we have centered our work of the first year on the single-link case.

The results of our research during this first year are presented in three reports. This first one is devoted to modelling and identification. The second one proposes a general control scheme and compares three specific controllers for the tip position. The third studies a control scheme to deal with changing payloads.

1.2. Introduction to Part I

First, we consider the problem of modelling a special class of single-link flexible arms: lumped-mass flexible arms. They consist of massless flexible structures that have some masses concentrated at certain points of the beam (see Figure 1). Only translations of these masses produce stresses in the flexible structure; their rotations do not generate any torque in the beam. So, the number of vibrational modes in the structure coincides with the number of lumped masses.

Little work has been done on the analysis and control of lumped-mass flexible structures. Book [7] studied the case of two rigid masses connected by a chain of massless beams having an arbitrary number of rotation joints. Our problem differs from this in the sense that our structure has only one rotation joint and an arbitrary number of lumped masses along the structure.

These particular structures are studied here because:

- Their dynamics may be modelled easily compared to distributed-mass flexible arms.
- Interesting properties for the control of flexible arms are deduced from their dynamic models.
- A method of easily controlling these arms is inferred from the structure of the model.
- The influence of changes in the tip's mass is easily characterized.
- Some robots and robot applications can be reasonably approximated by these models.
- Given a distributed-mass flexible arm, there always exists a truncated dynamic model which is of the same form as the lumped-mass flexible arm models, and which reproduces the dynamics of the

measured variables. This will allow us to generalize the above-mentioned control method to the case of distributed-mass flexible arms.

The influences of changes in the carried load are studied in this report. Results of this study allow us to tune the controllers to the particular payload, in order to keep the response of the system to changes in the position reference approximately invariant.

Section 2 establishes the dynamic model of these beams, some properties of the model are deduced in Section 3 that are useful in controlling these arms, and this modelling method is extended in Section 4 to the case of distributed-mass flexible beams.

A new method of identifying the dynamics of flexible arms in the presence of Coulomb friction (which is a strong nonlinearity) is developed in Section 5. It also provides an accurate estimate of the average value of the Coulomb friction over the range of working velocities. This method allows us to reconstruct the motor frequency response from experimental results, which are highly distorted by this nonlinear friction.

In Section 6 these methods are applied to a class of single-link lightweight flexible arms that we have designed in our laboratory for experimental purposes. These arms are very lightweight; they can perform quick movements, but the friction torque, which is comparable to the coupling torque between the motor and the beam, precludes the use of other existing identification and control methods. Experimental results are given for two of these arms.

Finally, conclusions are presented in Section 7.

2. Lumped-Mass Flexible Arm Modelling

We divide the model of our flexible arm into two submodels: the first one describes the behavior of the motor; the second one describes the behavior of the mechanical structure using the angle of the motor as its input. These two submodels are coupled by the reaction torque of the beam on the motor (see Figure 2). This model is quite different from the models normally used in the control of flexible arms, which consider the applied torque as the input to the beam (Truckenbrodt [8], Low [9]). Our model has some advantages when identifying flexible arms with friction in the joints [10] (explained in Section 5), and when trying to compensate for friction [11] (explained in Part II). We show here that another advantage of our model is that it allows us to separate the dynamic-model parameters that depend on the geometry of the beam from the parameters that depend on the lumped masses of the beam. Special attention is paid to this issue in this section because it will be used in the control design.

2.1. Beam modelling

Consider the system of Figure 1. It represents a massless flexible beam with n point masses distributed along the structure, the last mass being located at the tip of the beam. The inertia of the motor is included in the motor submodel. Let $m_i, 1 \leq i \leq n$ be the values of the masses and l_i the distances between consecutive masses $i-1$ and i, where l_1 is the distance between the rotation axis of the motor and the first mass. Let L_i be the distance between mass m_i and the axis of the motor. We assume that beam deflections are small enough so that the distances between masses m_i (measured along the length of the beam) are equal to the distances between the masses' projections on the x-axis.

We establish two coordinate systems, both with origins at the motor axis: the $\bar{x} - \bar{y}$ system is fixed in space, while the $x - y$ system moves with the motor shaft. Thus, the y-coordinate of a point represents the deflection of the point on the beam from its initially straight configuration, corresponding to the x-axis. We denote as $F(x)$ and $T(x)$ the force and torque, respectively, at this point: i.e. the force and torque acting on the beam just to the left of a point due to the action of the beam just to the right.

An external force, F_n, and torque, T_n, applied at the tip of the beam, are also considered in our model. F_n represents the component of the resultant applied force that is normal simultaneously to the beam and to the joint rotation velocity vector. T_n is the component of the resultant torque normal to the $x - y$ plane. These two quantitities represent the interaction of the beam with the environment and may be produced in several ways, a few of which are: they may be the reaction forces when following the contours of a surface, or the reaction of the next joint when dealing with a multilink arm; they may be produced by a load; they can even represent the small effects of friction on the tip (for example, in flexible arms mounted on an air table).

Assuming small deflections, a massless beam can be described by the static deflection relation:

$$E \cdot I \cdot \frac{d^4 y}{dx^4} = 0.$$

If the stiffness $E \cdot I$ is constant throughout each interval of the beam, the deflection in the interval $[i-1, i]$ is given by a third-order polynomial:

$$y_i(x) = u_{i,0} + u_{i,1} \cdot (x - L_{i-1}) + u_{i,2} \cdot (x - L_{i-1})^2 + u_{i,3} \cdot (x - L_{i-1})^3, \tag{1}$$

where $u_{i,j}$ are the polynomial coefficients, different in each interval, and $L_0 = 0$. We assume in the following analysis that $E \cdot I$ is constant throughout the beam.

2.1.1. Geometric equations

Imposing continuity conditions between two consecutive intervals up to the second derivative we get $3 \cdot (n-1)$ equations:

$$y_i(l_i) = y_{i+1}(0) \Rightarrow u_{i,0} + u_{i,1} \cdot l_i + u_{i,2} \cdot l_i^2 + u_{i,3} \cdot l_i^3 = u_{i+1,0}$$

$$\frac{dy_i}{dx}(l_i) = \frac{dy_{i+1}}{dx}(0) \Rightarrow u_{i,1} + 2 \cdot u_{i,2} \cdot l_i + 3 \cdot u_{i,3} . l_i^2 = u_{i+1,1} \tag{2}$$

$$\frac{d^2 y_i}{dx^2}(l_i) = \frac{d^2 y_{i+1}}{dx^2}(0) \Rightarrow u_{i,2} + 3 \cdot u_{i,3} \cdot l_i = u_{i+1,2}$$

for the joint between $[i-1, i]$ and $[i, i+1]$, $1 \leq i < n$. The continuity condition between the motor and the beam gives

$$y_1(0) = \frac{dy_1}{dx}(0) = 0 \Rightarrow u_{1,0} = 0, u_{1,1} = 0, \tag{3}$$

and the condition of the applied torque at the tip gives

$$T_n = E \cdot I \cdot \frac{d^2 y_n}{dx^2}(l_n) \Rightarrow u_{n,2} + 3 \cdot u_{n,3} \cdot l_n = \frac{T_n}{2 \cdot E \cdot I} \tag{4}$$

The set of geometrical equations is completed expressing deflections at specific points i in terms of these polynomials:

$$u_{i,0} + u_{i,1} \cdot l_i + u_{i,2} \cdot l_i^2 + u_{i,3} \cdot l_i^3 = y(L_i); \qquad 1 \leq i \leq n \tag{5}$$

2.1.2. Dynamic equations

If we apply Newton's equations to the n masses we get:

$$T(L_i) = \sum_{j=i+1}^{n} m_j \cdot (L_j - L_i) \cdot \frac{d^2 \hat{y}(L_j)}{dt^2} - T_n - F_n \cdot (L_n - L_i) \qquad 0 \leq i < n \tag{6}$$

$$F(L_i) = -\sum_{j=i+1}^{n} m_j \cdot \frac{d^2 \hat{y}(L_j)}{dt^2} + F_n \qquad 0 \leq i < n \tag{7}$$

where $\hat{y}(L_j)$ $(= y(L_j) + \theta_m \cdot L_j)$ is the arc position of mass j with respect to the $\tilde{x}$-axis (θ_m is the angle of the motor). Taking into account that

$$u_{i,2} = \frac{T(L_{i-1})}{2 \cdot E \cdot I}, \qquad u_{i,3} = -\frac{F(L_{i-1})}{6 \cdot E \cdot I} \tag{8}$$

and combining (6)-(8), we get

$$\frac{d^2 \hat{y}(L_i)}{dt^2} = \frac{6 \cdot E \cdot I}{m_i} \cdot (u_{i,3} - u_{i+1,3}); \qquad 1 \leq i \leq n \tag{9}$$

where $u_{n+1,3} = -\frac{F_n}{6 \cdot E \cdot I}$ is defined according to (8).

2.1.3. Dynamic model of the beam

Equations (2)-(5) allow us to express the coefficients $u_{i,j}$ as linear functions of $y(L_i)$ and T_n. $u_{i,3}$ coefficients can be expressed in a compact form:

$$\begin{pmatrix} u_{1,3} \\ u_{2,3} \\ \vdots \\ u_{n,3} \end{pmatrix} = \mathcal{U} \cdot \begin{pmatrix} y(L_1) \\ y(L_2) \\ \vdots \\ y(L_n) \\ T_n \end{pmatrix}, \tag{10}$$

where $\mathcal{U}$ is a constant matrix that depends only on the dimensions of the beam and the location of the masses.

Denoting as θ_i the angle between the $\bar{x}$-axis and the radial line from the origin to mass i (see Figure 1), taking into account that $\theta_i = \frac{y(L_i)}{L_i}$, and substituting (10) into (9), we get n linear equations of the form

$$\frac{m_i}{E \cdot I} \cdot \frac{d^2\theta_i}{dt^2} = \sum_{j=1}^{n} a_{i,j} \cdot \theta_j + b_i \cdot \theta_m + \frac{p_i}{E \cdot I} \cdot T_n \qquad 1 \leq i < n \tag{11}$$

$$\frac{m_n}{E \cdot I} \cdot \frac{d^2\theta_n}{dt^2} = \sum_{j=1}^{n} a_{n,j} \cdot \theta_j + b_n \cdot \theta_m + \frac{p_n}{E \cdot I} \cdot T_n + \frac{1}{L_n \cdot E \cdot I} \cdot F_n. \tag{12}$$

Equations (11) and (12) can be expressed in a compact form as:

$$\mathcal{M} \cdot \frac{d^2\Theta}{dt^2} = E \cdot I \cdot [\mathcal{A} \cdot \Theta + \mathcal{B} \cdot \theta_m] + \mathcal{P} \cdot T_n + \mathcal{Q} \cdot F_n, \tag{13}$$

where $\mathcal{M} = diag(m_1, m_2, \ldots, m_n)$, $\Theta^T = (\theta_1, \theta_2, \ldots, \theta_n)$, $\mathcal{A}$ is an $n \times n$ constant matrix, and $\mathcal{B}, \mathcal{P}$ and $\mathcal{Q}$ are constant $n \times 1$ column vectors. In particular, $\mathcal{Q}^T = (0, 0, \ldots, 0, L_n^{-1})$. In equation (13), $\mathcal{A}, \mathcal{B}, \mathcal{P}$ and $\mathcal{Q}$ depend only on the geometry of the beam. The values of the lumped masses only influence the matrix $\mathcal{M}$.

2.2. Motor modelling

The dynamic model for a D.C. motor is simple and can be written as:

$$K \cdot i = J \cdot \frac{d^2\theta_m}{dt^2} + V \cdot \frac{d\theta_m}{dt} + C_t + CF, \tag{14}$$

where K is the electromechanical constant of the motor, i is the current, J is the polar inertia of the motor, V is the dynamic friction coefficient, C_t is the coupling torque between motor and beam, and CF is the Coulomb friction. Taking into account that $C_t = -T(0) = -E \cdot I \cdot 2 \cdot u_{1,2}$, we can express this torque as a linear function:

$$C_t = \mathcal{H} \cdot \Theta + h_{n+1} \cdot \theta_m + h_{n+2} \cdot T_n, \tag{15}$$

where $\mathcal{H} = (h_1, h_2, \ldots, h_n)$, and $h_i, 1 \leq i \leq n+2$, are parameters that do not depend on the masses along

the beam.

3. Properties of the Lumped-Mass Model

The behavior of the flexible arm as described by equations (13)-(15) is represented in Figure 2. We assume that F_n and T_n are perturbations to the system. Then, in order to perform the analysis and design of the control system, we make $F_n = T_n = 0$. Some interesting properties of the lumped-mass model then follow:

1. From (13), using Laplace transforms we find that the transfer functions $\theta_i(s)/\theta_m(s) = G_i(s)$ for $1 \leq i \leq n$ have terms only of the form $s^{2-j}; 0 \leq j \leq n$, n being the number of lumped masses. Then the poles and zeros always come from factors of the form $(s^2 + z)$, z being a complex number in general, and the following cases are possible:

   a) $z \in \Re, z > 0 \Rightarrow$ two conjugate roots on the imaginary axis.

   b) $z \in \Re, z \leq 0 \Rightarrow$ two roots on the real axis, of the same magnitude but opposite sign.

   c) $z \in C, \Im(z) \neq 0 \Rightarrow$ sets of four symmetrical roots with respect to both real and imaginary axes.

   The mechanical structure is marginally stable because we assume there is no friction along the beam (no energy-dissipating phenomena), and the friction on the tip is treated as a perturbation. So the poles are always of case a). The zeros, however, may be of any of the three cases. Case b) appears quite often and produces non-minimum phase systems. Control of these systems presents some problems, as stated in [1].

2. The difference between the orders of the denominator and numerator of $G_i(s)$, $\forall i$, is at least two. This is a consequence of flexible arms. If the numerator and denominator were of the same order, it would mean that an instantaneous change in the position of the motor would produce an instantaneous change in the position of the ith point of the flexible arm (*Initial Value Theorem* of Laplace transforms; see Kuo [12]). This is not possible, however, because flexible beams need some time to propagate the motion along the structure.

3. *Separation Property.* It was mentioned in the previous section that the influence of the lumped masses on the dynamics of the arm may be perfectly separated from the influence of the geometrical dimensions of the beam (see equations (13) and (15)). This happens because the beam is modelled as massless; thus, its shape is given by static deflection equations that depend only on the position coordinates. This property is used in the controller design.

4. *Zeros Invariance Property.* Zeros of the $G_n(s)$ transfer function between the tip position θ_n and the angle of the motor θ_m remain constant independent of the payload of the tip. This is easily proved taking into account that:

$$\Theta = (\mathcal{M} \cdot s^2 - E \cdot I \cdot \mathcal{A})^{-1} \cdot E \cdot I \cdot \mathcal{B} \cdot \theta_m, \tag{16}$$

   and that the inverse of a square non-singular matrix A is given by $A^{-1} = \frac{adjA}{detA}$ ([13]). Then the nth row of $(\mathcal{M} \cdot s^2 - E \cdot I \cdot \mathcal{A})^{-1}$ is independent of m_n, as are the zeros of $G_n(s)$.

5. The perturbations F_n and T_n affect the dynamic behavior of all the masses of the beam structure linearly (equation (13)). F_n does not appear explicitly in (15); this is because the force applied to the tip does not appear in the geometric equations.

4. Extension to Distributed-Mass Flexible Arm Modelling

This section extends the proposed modelling method to the case of flexible arms with distributed masses. The following lemma is proposed:

Lemma: *Let us assume that:*

1. *There are no internal energy-dissipating phenomena in the structure of a distributed-mass flexible arm. Energy dissipation happens only in the joint in the form of friction. This means that property 1 of Section 3 remains true here. Property 2 is also true because the motion propagation from the base to the tip of the structure is not instantaneous.*
2. *The state space model of the distributed-mass flexible arm may be truncated, keeping in the model just the first few representative vibrational modes, and neglecting the other high-frequency modes. This truncation is always performed as a preliminary step in the design of controllers for flexible arms.*
3. *We measure the position at n points of the beam. We choose n equal to the number of vibrational modes considered in the truncated model of the beam, N_v.*

Then an equivalent lumped-mass flexible beam model:

$$\frac{d^2\Theta}{dt^2} = \hat{A} \cdot \Theta + \hat{B} \cdot \theta_m \tag{17}$$

$$C_t = \hat{\mathcal{H}} \cdot \Theta + \hat{h}_{n+1} \cdot \theta_m \tag{18}$$

can be defined that reproduces the dynamics of the distributed-mass flexible beam for the range of frequencies of interest.

This model represents the truncated dynamics of the distributed mass flexible beam. The external perturbations T_n and F_n were assumed to be 0 when deriving this model. Notice that now $\hat{A}$ and $\hat{B}$ depend on the distributed mass of the beam.

The following procedure is proposed to obtain this model from experimental measurements on a distributed-mass system.

Procedure.

1. Experimentally obtain the frequency response between the angle of the motor and the angle of the tip.
2. Fit a transfer function $\hat{G}_t(s)$ that relates the angle of the tip to the angle of the motor to this frequency data. This transfer function must exhibit properties 1 and 2 of Section 3. The order of the denominator divided by two is the number of vibrational modes N_v considered in the model.
3. Experimentally obtain the frequency responses, with respect to the angle of the motor, of other $(N_v - 1)$ points of the structure. No special conditions about the location of these points are required a priori.

4. Identify other $(N_v - 1)$ transfer functions $\hat{G}_i(s)$ from this data. The poles are common to the whole system, so these transfer functions will have the same denominator as $\hat{G}_t(s)$.

5. The portion of the model described by equation (17) may be obtained from these identified transfer functions $\hat{G}_1, \hat{G}_2, \hat{G}_3, \ldots, \hat{G}_{N_v-1}, \hat{G}_{N_v}$ (we denote $\hat{G}_t$ as $\hat{G}_{N_v}$) by the following procedure:

   Let $\Theta \in \Re^{N_v \times 1}$ be the column vector that represents the measured angles $\theta_1, \theta_2, \ldots, \theta_{N_v}$ at the selected points of the structure:

$$\hat{G}_i(s) = \frac{\begin{pmatrix} \mu_i & 0 \end{pmatrix} \cdot \mathcal{S}}{\delta \cdot \mathcal{S}}; \qquad 1 \leq i \leq N_v \tag{19}$$

   where $\mathcal{S}^T = \begin{pmatrix} 1 & s^2 & s^4 & \ldots & s^{2N_v} \end{pmatrix}, \qquad \mathcal{S} \in \Re^{N_v+1};$

   $\mu_i = \begin{pmatrix} \mu_{i,0} & \mu_{i,1} & \mu_{i,2} & \ldots & \mu_{i,N_v-1} \end{pmatrix}, \qquad \mu_i \in \Re^{N_v};$

   $\delta = \begin{pmatrix} \delta_0 & \delta_1 & \delta_2 & \ldots & \delta_{N_v-1} & 1 \end{pmatrix}, \qquad \delta \in \Re^{N_v+1}.$

   Notice that $\hat{G}_i$ is of this form because of properties 1 and 2 of Section 3.

   Then:

$$\frac{d^2\theta_i}{dt^2} = \frac{\begin{pmatrix} 0 & \mu_i \end{pmatrix} \cdot \mathcal{S}}{\delta \cdot \mathcal{S}} \cdot \theta_m(s). \tag{20}$$

   If $\hat{a}_{i,j}$ are the elements of $\hat{A}$, and $\hat{b}_i$ the elements of $\hat{B}$ in equation (17), then substituting (19)-(20) in (17) and identifying coefficients in the numerator we get:

$$\begin{pmatrix} 0 & \mu_i \end{pmatrix} = \sum_{j=1}^{N_v} \hat{a}_{i,j} \cdot \begin{pmatrix} \mu_j & 0 \end{pmatrix} + \hat{b}_i \cdot \delta.$$

   The coefficients of (17) are obtained from:

$$\hat{B}^T = (\mu_{1,N_v-1}, \mu_{2,N_v-1}, \ldots, \mu_{N_v,N_v-1}) \tag{21}$$

$$\hat{A} = \begin{pmatrix} \chi_1 \\ \chi_2 \\ \chi_3 \\ \vdots \\ \chi_{N_v} \end{pmatrix} \cdot \begin{pmatrix} \mu_1 \\ \mu_2 \\ \mu_3 \\ \vdots \\ \mu_{N_v} \end{pmatrix}^{-1}, \tag{22}$$

   where rows $\chi_i \in \Re^{1 \times N_v}$ are calculated from:

$$\begin{pmatrix} 0 & \mu_i \end{pmatrix} - \mu_{i,N_v-1} \cdot \delta = \begin{pmatrix} \chi_i & 0 \end{pmatrix}. \tag{23}$$

6. Expression (18) for the motor-beam coupling torque C_t may be obtained by the following steps:

   (a) Identification of the linear part of the dynamics of the motor: transfer function $\hat{G}_m(s) = \frac{\theta_m(s)}{i(s)}$.

   (b) Distortions in the identification because of the Coulomb friction may be avoided by using the procedure described in the next section.

(c) Denoting $C_t(s)$ by $\frac{n_c(s)}{d_c(s)} \cdot \theta_m(s)$ and substituting in (14) (after making $CF = 0$) we get:

$$K \cdot d_c(s) \cdot \hat{G}_m^{-1}(s) = (J \cdot s^2 + V \cdot s) \cdot d_c(s) + n_c(s).$$

And taking into account that $d_c(s) = \delta \cdot S$ (this is consequence of (15)), we determine J, V and $n_c(s)$. K is obtained from catalogue.

(d) Equation (18) is obtained from polynomials n_c and d_c by following an algebraic process similar to that shown in step 5 of the procedure for obtaining this model (page 10).

The only constraint to consider when choosing the $N_v - 1$ sensed points is that the numerators μ_i of the identified transfer functions at the N_v points should be linearly independent to permit inversion of the matrix that appears in (22). This means that very close points cannot be used for sensing.

A consequence of this section is that: *it is not necessary to build distributed-mass flexible arms in order to test control schemes for flexible arms. Lumped-mass flexible arms (which may be easier to build, model and identify) may be used in many cases as prototypes of real flexible arms, allowing us to test control laws on them before implementation in real arms.*

5. Parameter Identification in Cases Involving Coulomb Friction in the Joint

Several methods exist that identify transfer functions of dynamic systems. Because of the characteristic of flexible arms having sharp resonant frequencies in the normal range of operation, frequency methods seem to be better suited for identifying these systems, and have been used by many researchers [1,14]. However, they dealt with arms without friction in the joints. These methods can be easily extended to the case of linear dynamic friction, but they give erroneous results when the Coulomb friction is significant. This is because they are based on linear models, but the Coulomb friction is nonlinear.

In this section we develop a new method of identifying flexible arms that extends the frequency identification techniques to cases involving Coulomb friction.

The dynamics of the joint are given by equations (14) and (15). The coupling torque $C_t(t)$ is related to the angle $\theta_m(t)$ by a linear differential equation (or transfer function) obtained by assuming $T_n = F_n = 0$, using Laplace transforms, and substituting Θ of (13) in (15). The term $CF(t)$ is related to the velocity of the motor.

Several models have been proposed to describe the friction of a DC motor, taking into account its linear and nonlinear quantities (a recent review may be found in [15]). The Coulomb friction is the most important quantity in all of them. This is especially true when dealing with direct-drive arms because the range of motor speeds is relatively low and, consequently, the dynamic friction is also low. The dynamic friction may be modelled as a first approximation by a linear term proportional to the speed of the motor, and the Coulomb friction CF by a constant whose sign changes with the sign of the velocity of the motor. Thus we use the following friction model:

$$\textit{Friction torque} = CF + V \cdot \frac{d\theta_m(t)}{dt} \qquad \dot{\theta}_m(t) > 0$$

$$\textit{Friction torque} = -CF + V \cdot \frac{d\theta_m(t)}{dt} \qquad \dot{\theta}_m(t) < 0$$

This simple model is a good description of the friction in many cases. The identification method that

we propose provides an averaged value of all the parameters (either friction or linear dynamics parameters) of the arm because it uses the spectral characteristics of the input and output signals.

The proposed identification method is divided into three stages [10]. First, a high-gain position loop is established around the motor in order to make it follow the reference position closely. The achievement of this allows us to know the velocity of the motor and hence the shape of the temporal evolution of the Coulomb friction. Then get the magnitude of the Coulomb friction from this shape and from the spectral analysis of the measured signals. Finally, this value is used to correct the experimental measurements of the frequency response of the motor, which are distorted by this nonlinear friction term.

5.1. Control of Motor Position

The first stage of our proposed identification method is to design a closed-loop control system around the position of the motor in order to force it to follow a specified trajectory. The design of this control system is straightforward, and a normal proportional-plus-derivative (*PD*) controller may be used for this purpose. If we apply a sinusoidal reference trajectory to the closed-loop system, the angular velocity of the motor will be approximately sinusoidal. The motor current will reflect both the torque needed to drive the motor and beam (i.e. all the linear terms) and the torque needed to overcome the Coulomb friction, which is ideally a square wave in phase with the velocity of the motor. The magnitude of the Coulomb friction remains to be determined. The block diagram of the identification setup is shown in Figure 3.

5.2. Calculation of Magnitude of Coulomb Friction

Assume that the closed-loop position control system for the motor is excited with a sinusoidal reference signal of frequency ω_0. If the system were linear, we would find that the current and the angle of the motor would be represented by sinusoidal functions of the same frequency. Because of the nonlinearity present in the system, however, the current will not be sinusoidal. Performing a spectral analysis of the position and current signals ([16], e.g.), we find:

1. The motor position has a peak at frequency ω_0, with no other significant peak.
2. The motor current has a dominant peak at frequency ω_0, and other peaks of smaller but not negligible magnitude at frequencies $3 \cdot \omega_0, 5 \cdot \omega_0, 7 \cdot \omega_0, \ldots$.

An explanation of the second phenomenon concerning current may be given in terms of the Fourier series expansion of the Coulomb friction torque, represented by a square wave of frequency ω_0. The Fourier series of a square wave can be written as

$$CF(t) = \sum_{i=1}^{\infty} A_i \cdot cos(i \cdot \omega_0 \cdot t + \phi), \tag{24}$$

where

$$A_i = \frac{2 \cdot CF}{i \cdot \pi} \cdot (1 - (-1)^i), \tag{25}$$

CF is the magnitude of the Coulomb friction torque, and ϕ is the phase angle of each harmonic, which in this case is equal to 0 $\forall i$ (all the harmonics are in phase with the fundamental wave).

Equation (25) indicates that Coulomb friction generates odd harmonics of the fundamental frequency ω_0. Because these harmonics appear on the right hand-side of equation (14) and the angle of the motor does not contain these harmonics, the current i which appears on the left hand-side of equation (14) must contain these harmonics.

Using equation (25), we can now determine the magnitude of CF, based on the study of the third harmonic.

If the system is excited with frequency ω_0, then in equation (14), the fundamental component of the current is given by

$$i_1(\omega_0) = G^{-1}(\omega_0) \cdot \theta_m(\omega_0) + j \cdot \frac{4 \cdot CF}{K \cdot \pi} \cdot e^{j \cdot \angle \theta_m(\omega_0)}, \tag{26}$$

where $i_1(\omega_0)$ is the polar representation of the first harmonic of the current at ω_0, $G(\omega_0)$ is the frequency characteristic function of the linear part of the motor model at frequency ω_0, and $\angle\theta$ is the phase of θ. Notice that the term $j \cdot e^{j \cdot \angle \theta_m(\omega_0)}$ is added to express that the Coulomb friction leads the motor position by 90 degrees; i.e., it is in phase with the velocity of the motor.

Also with the system driven at ω_0, the third harmonic of the current is given by

$$i_3(3 \cdot \omega_0) = G^{-1}(3 \cdot \omega_0) \cdot \theta_{m3}(3 \cdot \omega_0) + j \cdot \frac{4 \cdot CF}{3 \cdot K \cdot \pi} \cdot e^{j \cdot \angle \theta_m(\omega_0)}. \tag{27}$$

While $\theta_{m3}(3 \cdot \omega_0)$ is close to zero for arms without any flexibility, this is not the case for flexible arms. When $3 \cdot \omega_0$ is close to one of the natural frequencies of the beam, the position control system is unable to completely compensate for the varying beam torque due to the oscillations that are excited at that frequency. The control system does eliminate these oscillations sufficiently for us to consider that the motor position still closely follows a sinusoid of frequency ω_0 and thus equations (24) and (25) approximately valid. However, the small high-frequency ripple that θ_m now presents should be considered in equation (27) because the factor $G^{-1}(3 \cdot \omega_0)$ is very high ($G(j \cdot \omega) = 0$ at the beam resonant frequencies).

We repeat this experiment now using a sinusoid signal of frequency $3 \cdot \omega_0$ as a reference for the motor position. This time we get the fundamental component of the current as

$$i_1(3 \cdot \omega_0) = G^{-1}(3 \cdot \omega_0) \cdot \theta_m(3 \cdot \omega_0) + j \cdot \frac{4 \cdot CF}{K \cdot \pi} \cdot e^{j \cdot \angle \theta_m(3 \cdot \omega_0)} \tag{28}$$

Equations (27) and (28) constitute a system of two complex equations with two unknown complex parameters, $G^{-1}(3 \cdot \omega_0)$ and CF. In theory, the value CF should be real, but because of small errors in the measurements, it was found to have a small imaginary component. In order to get the real number CF that gives the best approximation for equations (27) and (28), an algorithm that minimizes the following cost function was implemented:

$$Cost = ln^2(|\ CF'/CF\ |) + (\angle CF')^2, \tag{29}$$

where CF' is defined from CF as follows:

1. For a given value of the Coulomb friction CF, obtain $G^{-1}(3 \cdot \omega_0)$ from (28).
2. For the above G^{-1}, obtain CF' from (27).

In other words, a function is defined between CF and its associated cost according to the scheme:

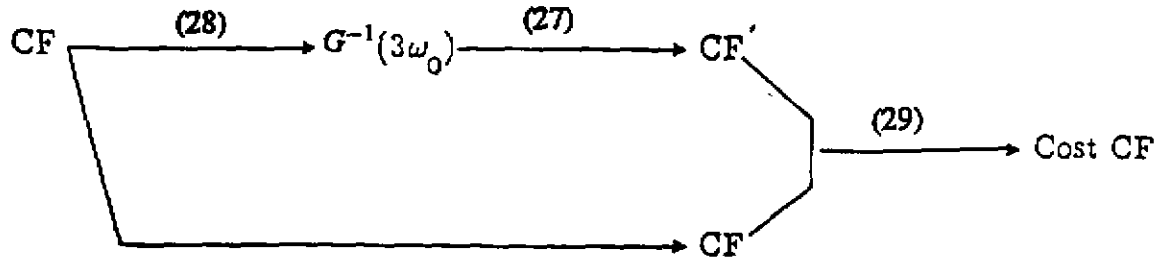

The value of CF that minimizes this cost function was obtained using a simple direct search method. Notice that (29) represents the magnitude of the ratio $ln(\frac{CF'}{CF})$, which is a complex number. This cost function was chosen to give equal weight to errors in magnitude and phase.

Different values of CF must be obtained for different frequencies, and the average of them must be taken as the estimated value for the Coulomb friction. This is because the values of CF may differ considerably depending on ω_0 (we had variations of 20% around the mean value in our experiments).

5.3. Correction of Frequency Data

Once the mean value of the Coulomb friction is obtained, the frequency response of the linear part of the model of the motor, $G(\omega)$, can be expressed (from equation (26)) as:

$$G(\omega) = \frac{\theta_m(\omega)}{i(\omega) - j \cdot \frac{4 \cdot CF}{K \cdot \pi} \cdot e^{j \cdot \angle \theta_m(\omega)}} \tag{30}$$

Equation (30) is solved using the experimental data obtained previously for the current $i(\omega)$ and the angle of the motor $\theta_m(\omega)$.

Therefore, we have obtained the corrected experimental frequency data and an average value for the Coulomb friction. Now a transfer function may be fitted to this data. This transfer function gives the relationship between the current and the angle of the motor.

Also obtained from the experimental data was the transfer function between the angle of the motor and the angle of the tip. This way of representing the dynamics of the system is quite different from the way used in the other approaches, in which relations between current and angle of the motor, and between current and angle of the tip are established. These two last relations are influenced by the Coulomb friction, and the measurements taken to identify them are therefore distorted by this nonlinear quantity. Our representation has the advantage that identifying the transfer function between the angle of the motor and the angle of the tip produces a very clean transfer function that is independent of motor friction. Consequently, nonlinear terms are not present, allowing the use of conventional frequency identification methods to obtain the dynamics of the beam.

6. Examples and Experimental Results

6.1. Experimental Setup

The mechanical system consists of a DC motor, a slender arm attached to the motor hub, and a mass at the end of the arm floating on an air table. Figure 4 shows the major parts of the system. Optionally, masses at intermediate locations of the beam may be added.

Figure 5 shows the arrangement of the single-mass beam used in the first example. In this case, the arm is a piece of music wire (7 *inches* long and 0.032 *inches* in diameter) clamped to the motor hub. The tip mass is a 1/16-*inch* thick, 5 3/4-*inch* diameter fiberglass disk attached at its center to the end of the beam with a freely pivoting pin joint. The disk has a mass of 54 *grams* and floats on the horizontal air table with minimal friction. Because the mass of the beam is small compared to that of the disk, and because the pin joint prevents generation of torque at the end of the beam, this mechanical system behaves practically like an ideal, undamped mass-spring system, being a minimum phase system.

In the second example, the wire is replaced by a longer one, and two masses are attached, one at the middle, and the other at the end of the wire. The second system has the characteristics of flexible arms with distributed mass, being a non-minimum phase system.

An Inland direct-drive motor drives the arm. The amplifier current limit is set at 4.12 *amp*, which corresponds to a 9.0 *lb.inch* motor torque. The Coulomb friction of the motor is about .288 *lb.inch* (corresponding to .132 *amp*) and has a significant effect on the control when the torque to the arm is low, as with our very slender arms.

Two sensors are used for the control of the system. A 7/8-*inch*, 360-*degree* potentiometer measures the angle of the motor shaft. A Hamamatsu tracking camera senses the x-y position of an infrared LED mounted on the tip of the arm in the case of the single-mass flexible arm. In the case of the two-mass flexible arm, a Selspot tracking camera is used that simultaneously senses the position of two infrared LED's mounted on the two masses of the arm.

The control algorithm was implemented on an Omnibyte OB68K1A, MC 68000-based computer with 512 Kbytes dynamic RAM and a 10-MH clock. Because the control computer is relatively slow, real-time computations were done in integer or short integer mode. Analog interfacing was provided with 12-bit

A/D and D/A boards. The sampling period used to control both arms was 3 *msec*.

6.2. Single-Mass Flexible Arm

6.2.1. Modelling

This is the simplest case. Following the procedure in Section 2, we have:

Geometric equations:

- There is no equation (2).
- Equation (3): $u_{1,0} = u_{1,1} = 0$.
- Equation (4): $u_{1,2} + 3 \cdot l_1 \cdot u_{1,3} = \frac{T_1}{2 \cdot E \cdot I}$.
- Equation (5): $u_{1,0} + l_1 \cdot u_{1,1} + l_1^2 \cdot u_{1,2} + l_1^3 \cdot u_{1,3} = y(L_1)$

Dynamic equations:

- Equation (9): $l_1 \cdot \frac{d^2\theta_1}{dt^2} = \frac{6 \cdot E \cdot I}{m_1} \cdot (u_{1,3} + \frac{F_1}{6 \cdot E \cdot I})$

Dynamic model of the beam:

- Equation (10): $u_{1,3} = \underbrace{\begin{pmatrix} -\frac{1}{2 \cdot l_1^3} & \frac{1}{4 \cdot l_1 \cdot E \cdot I} \end{pmatrix}}_{U} \cdot \begin{pmatrix} y(L_1) \\ T_1 \end{pmatrix}$.
- Substituting $y(L_1) = l_1 \cdot (\theta_1 - \theta_m)$ in the above equation, and combining it with the dynamic equation, we obtain equation (13):

$$m_1 \cdot \frac{d^2\theta_1}{dt^2} = E \cdot I \cdot [-\frac{3}{l_1^3} \cdot \theta_1 + \frac{3}{l_1^3} \cdot \theta_m] + \frac{3}{2 \cdot l_1^2} \cdot T_1 + \frac{1}{l_1} \cdot F_1 \tag{31}$$

Dynamic model of the motor:

- We use (14) as it is.
- Coupling torque (15):

$$C_l = -2 \cdot E \cdot I \cdot u_{1,2} = 6 \cdot E \cdot I \cdot l_1 \cdot u_{1,3} - T_1 = -\frac{3 \cdot E \cdot I}{l_1} \cdot \theta_1 + \frac{3 \cdot E \cdot I}{l_1} \cdot \theta_m + \frac{1}{2} \cdot T_1 \tag{32}$$

There is dynamic friction between the air table and the disk. Therefore, $F_1 = -\nu \cdot \frac{d\theta_1}{dt}$, ν being the friction coefficient. Assuming $T_1 = 0$, and substituting the mechanical parameters $E = 30 \cdot 10^6$ $lb/in.^2$, $I = \frac{\pi \cdot 0.032^4}{64}$ $in.^4$, $m_1 = 0.121$ $lb.$, and $l_1 = 7$ $in.$ in equations (31) and (32), we get:

$$\frac{\theta_1(s)}{\theta_m(s)} = \frac{43.1}{s^2 + 1.18 \cdot \nu \cdot s + 43.1} \tag{33}$$

$$C_t = 0.662 \ \ lb.in./rad. \cdot (\theta_m - \theta_1) \tag{34}$$

6.2.2. Identification

Transfer functions of the motor and beam were obtained using the method described in Section 5. Figures 6 and 7 show the frequency responses of motor and beam, respectively. The transfer function fitted to the corrected data of the motor was:

$$\frac{\theta_m(s)}{i(s)} = \frac{394.94 \cdot (s^2 + 0.06 \cdot s + 43.75)}{s \cdot (s^3 + 2.26 \cdot s^2 + 165.7 \cdot s + 103.56)} \tag{35}$$

The transfer function fitted to the data of the beam was:

$$g_1(s) = \frac{43.75}{s^2 + 0.06 \cdot s + 43.75}. \tag{36}$$

From these transfer functions, the following parameters were obtained:

Parameters of equation (14):

$J = 0.005529 \ lb.in.sec^2$
$V = 0.01216 \ lb.in./rad./sec.$
$K = 2.184 \ lb.in./amp.$ (value obtained from catalogue)
$CF/K = 0.132 \ amp.$

Equation (15) gives:

$$C_t = 0.674 \ \ lb.in./rad. \cdot (\theta_m - \theta_1). \tag{37}$$

Equation (13) gives:

$$0.12136 \cdot \frac{d^2\theta_1}{dt^2} = -5.3095 \cdot \theta_1 + 5.3095 \cdot \theta_m - 0.0072816 \cdot \frac{d\theta_1}{dt},$$

where the last term on the right-hand side of the equation represents the perturbation because of the friction between the disk attached to the arm tip and the air table: $\nu = 0.051 \ lb.sec./rad.$

Comparing (33)-(34) with (36)-(37), we see that errors between theoretical and identified parameters are less than 2%. So, the mechanical model of the beam may be accurately obtained from the theoretical parameters obtained by using the equations in Section 2.

Parameters J and K of equation (14) can be obtained from a catalogue, but V and CF have to be experimentally estimated. Figure 8 shows friction characteristics of the motor obtained by using the classical method of plotting the motor velocity versus the current needed by the motor to run at steady velocity. Because of the stiction present in the system, the values of the currents at low velocities could not be obtained. Using a linear extrapolation of the experimental data given in Figure 8, the value of the current required for the Coulomb friction torque was found to be 0.161 *amp* for the positive velocity and 0.152 *amp* for the negative velocity. These values are different from the value obtained from the proposed spectral method. Some motor control experiments, which will be described in Part II, showed that the value estimated from our method was more accurate than these values obtained from the classical method. This is because Coulomb and dynamic frictions are estimated in the classical method by extrapolating from high-speed measurements that are outside the working range of velocities of this motor, while in our method these values are estimated from low-velocity measurements inside this range.

6.3. Two-Mass Flexible Arm Modelling

We develop in this subsection the equations of the beam shown in Figure 9, and the coupling between motor and beam. Identification is not done here because: 1) the parameters of equation (14), including Coulomb friction, remain the same as in the previous example because here we use the same motor; 2) in the previous subsection we showed that differences between experimental and theoretical beam transfer functions are small. Thus, the beam transfer function can be accurately obtained by modelling the mechanical system.

Now again following the procedure in Section 2, we obtain:

Geometric equations:

- Equations (2):

$$u_{1,0} + u_{1,1} \cdot l_1 + u_{1,2} \cdot l_1^2 + u_{1,3} \cdot l_1^3 = u_{2,0}$$

$$u_{1,1} + 2 \cdot u_{1,2} \cdot l_1 + 3 \cdot u_{1,3} \cdot l_1^2 = u_{2,1}$$

$$u_{1,2} + 3 \cdot u_{1,3} \cdot l_1 = u_{2,2}$$

- Equation (3): $u_{1,0} = u_{1,1} = 0.$
- Equation (4): $u_{2,2} + 3 \cdot l_2 \cdot u_{2,3} = \frac{T_2}{2 \cdot E \cdot I}.$

- Equations (5):

$$u_{1,0} + l_1 \cdot u_{1,1} + l_1^2 \cdot u_{1,2} + l_1^3 \cdot u_{1,3} = y(L_1)$$

$$u_{2,0} + l_2 \cdot u_{2,1} + l_2^2 \cdot u_{2,2} + l_2^3 \cdot u_{2,3} = y(L_2)$$

Dynamic equations:

- Equations (9):

$$l_1 \cdot \frac{d^2\theta_1}{dt^2} = \frac{6 \cdot E \cdot I}{m_1} \cdot (u_{1,3} - u_{2,3})$$

$$(l_1 + l_2) \cdot \frac{d^2\theta_2}{dt^2} = \frac{6 \cdot E \cdot I}{m_2} \cdot (u_{2,3} + \frac{F_2}{6 \cdot E \cdot I})$$

Dynamic model of the beam:

- Equation (10):

$$\begin{pmatrix} u_{1,3} \\ u_{2,3} \end{pmatrix} = \mathcal{U} \cdot \begin{pmatrix} y(L_1) \\ y(L_2) \\ T_2 \end{pmatrix}, \tag{38}$$

where

$$\mathcal{U} = \frac{1}{l_1 \cdot l_2 \cdot (3 \cdot l_1 + 4 \cdot l_2)} \cdot \begin{pmatrix} -\frac{3 \cdot l_1^2 + 6 \cdot l_1 \cdot l_2 + 2 \cdot l_2^2}{l_1^2} & 3 & -\frac{l_2^2}{2 \cdot E \cdot I} \\ \frac{2 \cdot l_1 + 3 \cdot l_2}{l_2} & -\frac{2 \cdot l_1}{l_2} & \frac{l_1 \cdot (l_1 + 2 \cdot l_2)}{2 \cdot E \cdot I} \end{pmatrix}.$$

- Substituting $y(L_1) = l_1 \cdot (\theta_1 - \theta_m), y(L_2) = (l_1 + l_2) \cdot (\theta_2 - \theta_m)$ in the above equation, and combining it with the dynamic equations, we obtain equation (13):

$$\mathcal{M} \cdot \begin{pmatrix} \frac{d^2\theta_1}{dt^2} \\ \frac{d^2\theta_2}{dt^2} \end{pmatrix} = E \cdot I \cdot [\mathcal{A} \cdot \begin{pmatrix} \theta_1 \\ \theta_2 \end{pmatrix} + \mathcal{B} \cdot \theta_m] + \mathcal{P} \cdot T_2 + \mathcal{Q} \cdot F_2, \tag{39}$$

where

$$\mathcal{M} = \begin{pmatrix} m_1 & 0 \\ 0 & m_2 \end{pmatrix}, \qquad \mathcal{P} = \frac{6}{l_1^2 \cdot l_2 \cdot (3 \cdot l_1 + 4 \cdot l_2)} \cdot \begin{pmatrix} -(l_1 + l_2)^2/2 \\ \frac{l_1^2 \cdot (l_1 + 2 \cdot l_2)}{2 \cdot (l_1 + l_2)} \end{pmatrix}, \qquad \mathcal{Q} = \begin{pmatrix} 0 \\ \frac{1}{l_1 + l_2} \end{pmatrix},$$

$$\mathcal{A} = \frac{6}{l_1^2 \cdot l_2 \cdot (3 \cdot l_1 + 4 \cdot l_2)} \cdot \begin{pmatrix} -(6 \cdot l_1 + 6 \cdot l_2 + 2 \cdot \frac{l_2^2}{l_1} + 2 \cdot \frac{l_1^2}{l_2}) & (l_1 + l_2) \cdot (3 + 2 \cdot \frac{l_1}{l_2}) \\ \frac{(2 \cdot l_1 + 3 \cdot l_2) \cdot l_1^2}{l_2 \cdot (l_1 + l_2)} & -2 \cdot l_1^2 / l_2 \end{pmatrix},$$

and

$$\mathcal{B} = \frac{6}{l_1^2 \cdot l_2 \cdot (3 \cdot l_1 + 4 \cdot l_2)} \cdot \begin{pmatrix} l_1 + 3 \cdot l_2 + 2 \cdot \frac{l_2^2}{l_1} \\ -l_1^2 / (l_1 + l_2) \end{pmatrix}.$$

Coupling torque (15):

$$C_t = -2 \cdot E \cdot I \cdot u_{1,2} = 2 \cdot E \cdot I \cdot l_1 \cdot u_{1,3} - \frac{2 \cdot E \cdot I \cdot y_1}{l_1^2}$$

$$= \mathcal{H} \cdot \begin{pmatrix} \theta_1 \\ \theta_2 \end{pmatrix} + \frac{12 \cdot E \cdot I \cdot (l_1 + l_2)}{l_1 \cdot (3 \cdot l_1 + 4 \cdot l_2)} \cdot \theta_m - \frac{l_2}{(3 \cdot l_1 + 4 \cdot l_2)} \cdot T_2, \tag{40}$$

where

$$\mathcal{H} = \frac{6 \cdot E \cdot I \cdot (l_1 + l_2)}{l_2 \cdot (3 \cdot l_1 + 4 \cdot l_2)} \cdot \begin{pmatrix} -(1 + 2 \cdot \frac{l_2}{l_1}) & 1 \end{pmatrix}.$$

Substituting the mechanical parameter: $E = 30 \cdot 10^6\ lb/in.^2, I = \frac{\pi \cdot 0.047^4}{64}\ in.^4, m_1 = m_2 = 0.121\ lb., l_1 = l_2 = 6\ in.$ in equations (39) and (40), we get:

$$\mathcal{M} = \begin{pmatrix} 0.12136 & 0 \\ 0 & 0.12136 \end{pmatrix}; \quad \mathcal{A} = \begin{pmatrix} -176.6032 & 110.377 \\ 27.59425 & -22.0754 \end{pmatrix} \quad \mathcal{B} = \begin{pmatrix} 66.2262 \\ -5.51885 \end{pmatrix}$$

$$\mathcal{P} = \begin{pmatrix} -0.047619 \\ 0.017857 \end{pmatrix}; \quad \mathcal{Q} = \begin{pmatrix} 0 \\ 0.0833 \end{pmatrix} \quad \mathcal{H} = \begin{pmatrix} -6.159 \\ 2.053 \end{pmatrix} \quad h_3 = 4.106, h_4 = -0.1429.$$

Assuming $T_2 = F_2 = 0$, we obtain from (39) the following transfer functions:

$$\frac{\theta_1(s)}{\theta_m(s)} = \frac{545.7 \cdot (s^2 + 106.10833)}{s^4 + 1637.1 \cdot s^2 + 57903.3175} \tag{41}$$

$$\frac{\theta_2(s)}{\theta_m(s)} = \frac{-45.465 \cdot (s^2 - 1273.3)}{s^4 + 1637.1 \cdot s^2 + 57903.3175} \tag{42}$$

Theoretical natural frequencies of the beam were obtained from the poles of these transfer functions. They are: 6.014 *rad./sec.* and 40.0116 *rad./sec.*. These frequencies were later measured experimentally, and differences between them and these theoretical values were smaller than 5%. Finally, notice that the last transfer function (equation (42)) is non-minimum phase exhibiting a positive zero at the theoretical position of 35.683.

7. Summary and Conclusions

This report has discussed the modelling and identification of single-link flexible arms with lumped masses. Most flexible arms have their mass distributed along all the structure, but there are some applications in which a model using lumped masses may be useful. A typical example is the case of a lightweight flexible arm carrying a heavy load. Here, only one vibrational mode is normally important, allowing approximate modelling by a massless beam with a mass attached to the tip. Another reason to study flexible arms with lumped masses is that some properties and control methods for these systems may be easily extended to the distributed mass case.

A new way of modelling these systems was presented in Section 2. In order to deal with nonlinear Coulomb friction, two submodels have been defined: one that describes the behavior of the motor and includes friction nonlinearities, and another linear submodel that describes the mechanical behavior of the beam. Both submodels are coupled by the torque at the base of the beam. In order to make the model more general, perturbations in the tip, represented by a torque and a force, have been considered. These perturbations allow us to consider the effects on the model of friction in the tip, changes in the carried load, or reaction forces produced by the next joint (in the case of a multiple-link flexible arm).

Some properties were deduced from these dynamical models in Section 3. The most interesting one is the *Separation Property*, which defines the influence of the masses on the beam. It permits representing the product of the mass i and its angular acceleration by a linear combination of the deflections of the beam at the points where there are masses. This linear combination depends only on the geometry of the beam.

Modelling was generalized in Section 4 to the distributed-mass flexible arm case. Using the identification procedure described in Section 4, the dynamics of distributed-mass flexible arms may be represented by models of the same form as those represented by equations (13)-(15). Another conclusion drawn from this section is that equivalent lumped-mass flexible arms may be used as prototypes of real flexible arms in order to test control laws. This section does not make any statement about the influence of the tip mass on the dynamics of the system. It seems that distributed-mass flexible arms may be considered as the limit of lumped-mass flexible arms when $n \rightarrow \infty$. But analytical proof of this has not been provided yet. If it is true, then properties of Section 3 (which describe the influence of the tip mass on the model) remain valid in the distributed-mass case. Further work is needed to verify this.

Section 5 described a new method of identifying the linear part of the model of a motor in the presence of Coulomb friction (motor submodel of a flexible arm, described by equations (14)-(15)). In this method, the Coulomb friction of the motor is obtained from frequency data instead of temporal data, as is the case in other existing methods. The proposed method presents two advantages: 1) Coulomb friction is estimated for the normal range of velocities at which the arm is operating, whereas the other methods estimate the Coulomb friction by extrapolating from high-speed measurements; 2) the proposed method gives an average value of the Coulomb friction over a range of velocities, whereas the other methods determine the friction only at certain speeds. This method may be applied to any DC motor.

Finally, some modelling and experimental identification results were presented in Section 6. Modelling has been applied to two lumped-mass flexible arms that we have built in our laboratory. The first one is a minimum phase single-mass flexible arm, while the second is a non-minimum phase two-mass flexible arm. The identification method has been applied to the single-mass flexible arm, and to the DC motor, which is common to both arms. Experimental results agreed with the theoretical model.

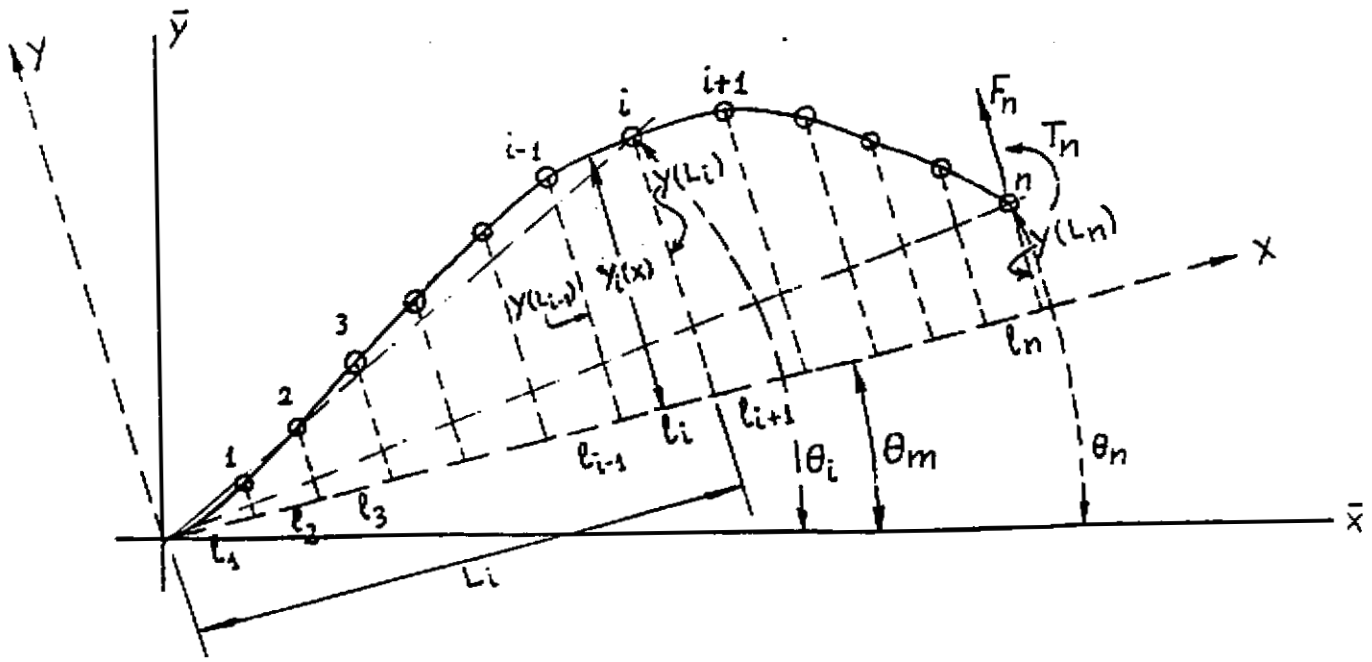

Figure 1: Lumped-mass flexible beam.

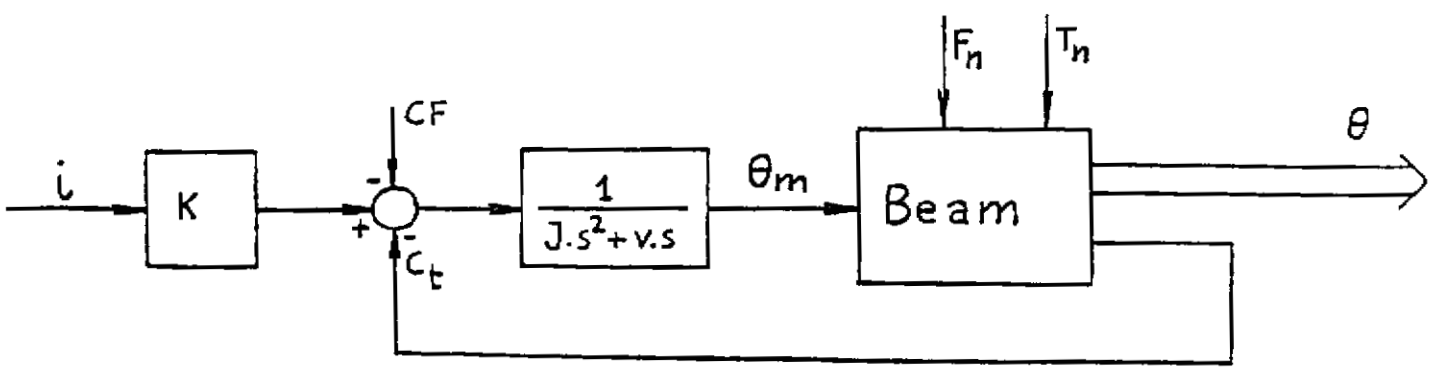

Figure 2: Dynamic model of the arm.

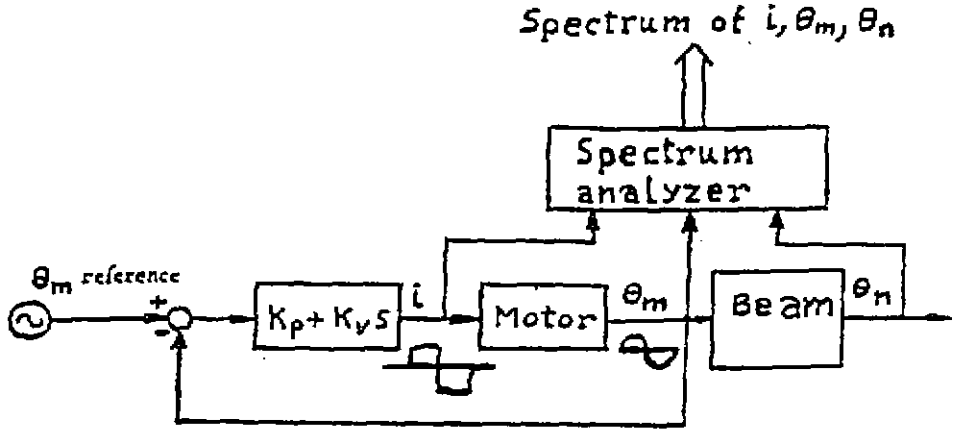

Figure 3: Identification setup.

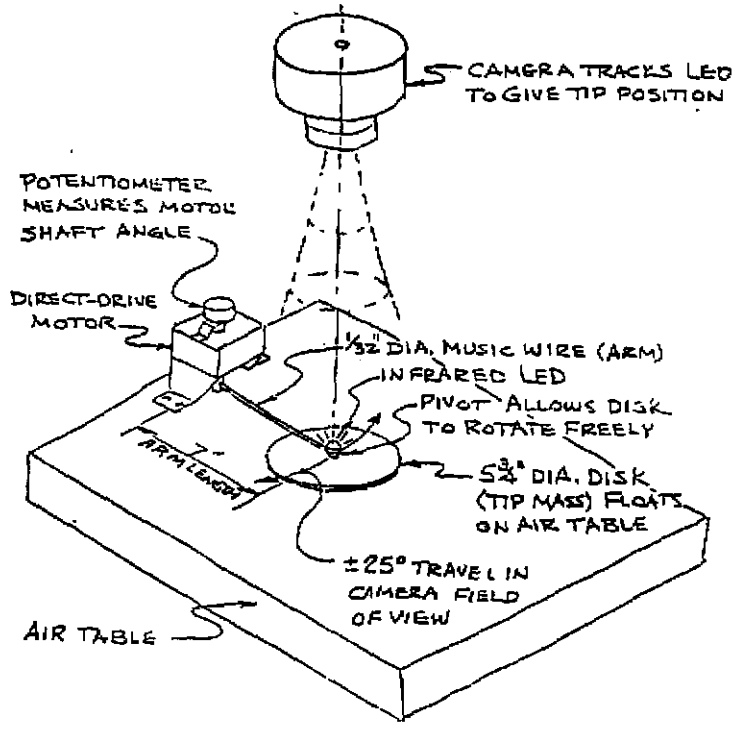

Figure 4: Experimental setup of the single-mass flexible beam.

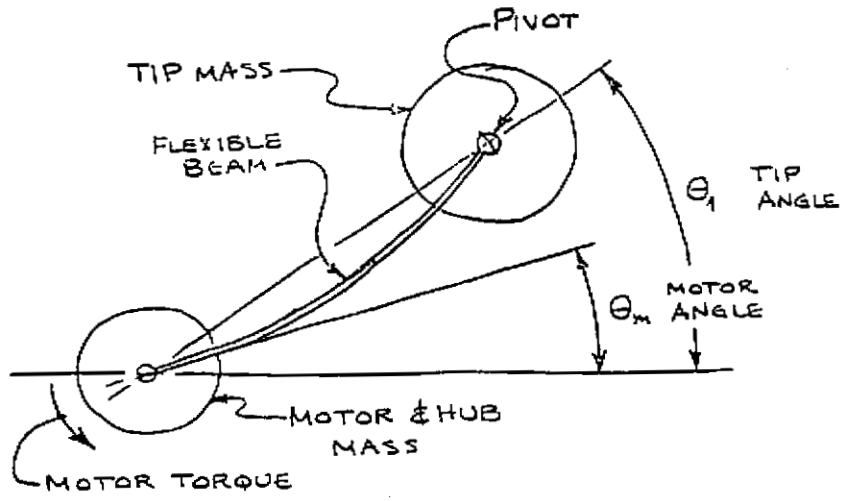

Figure 5: System nomenclature for the single-mass arm.

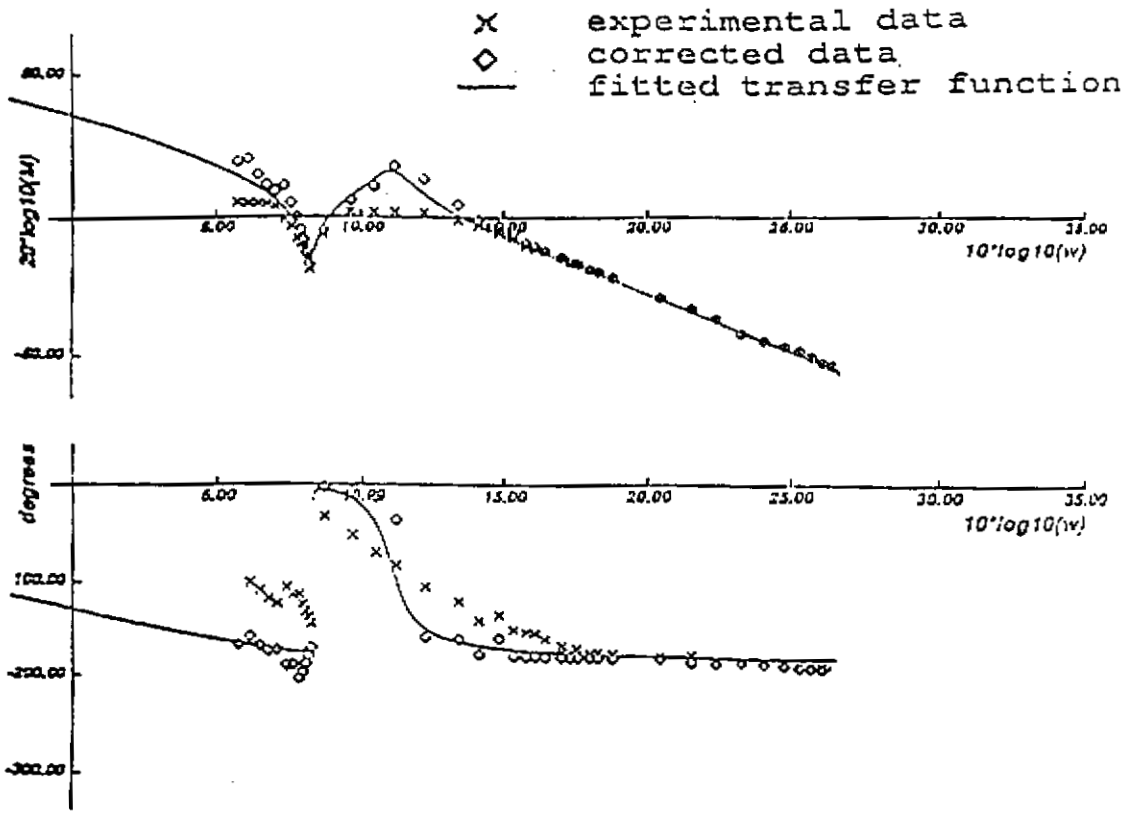

Figure 6: Frequency characteristics of the motor submodel (including coupling with the beam).

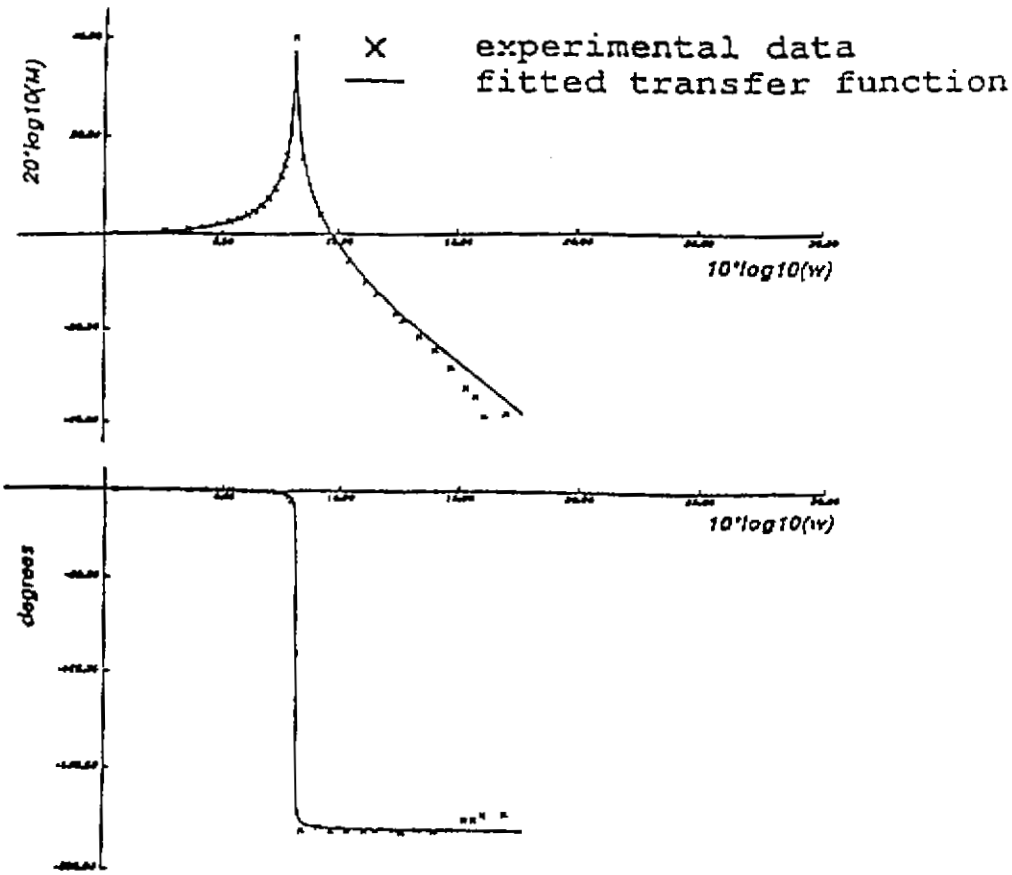

Figure 7: Frequency characteristics of the beam submodel.

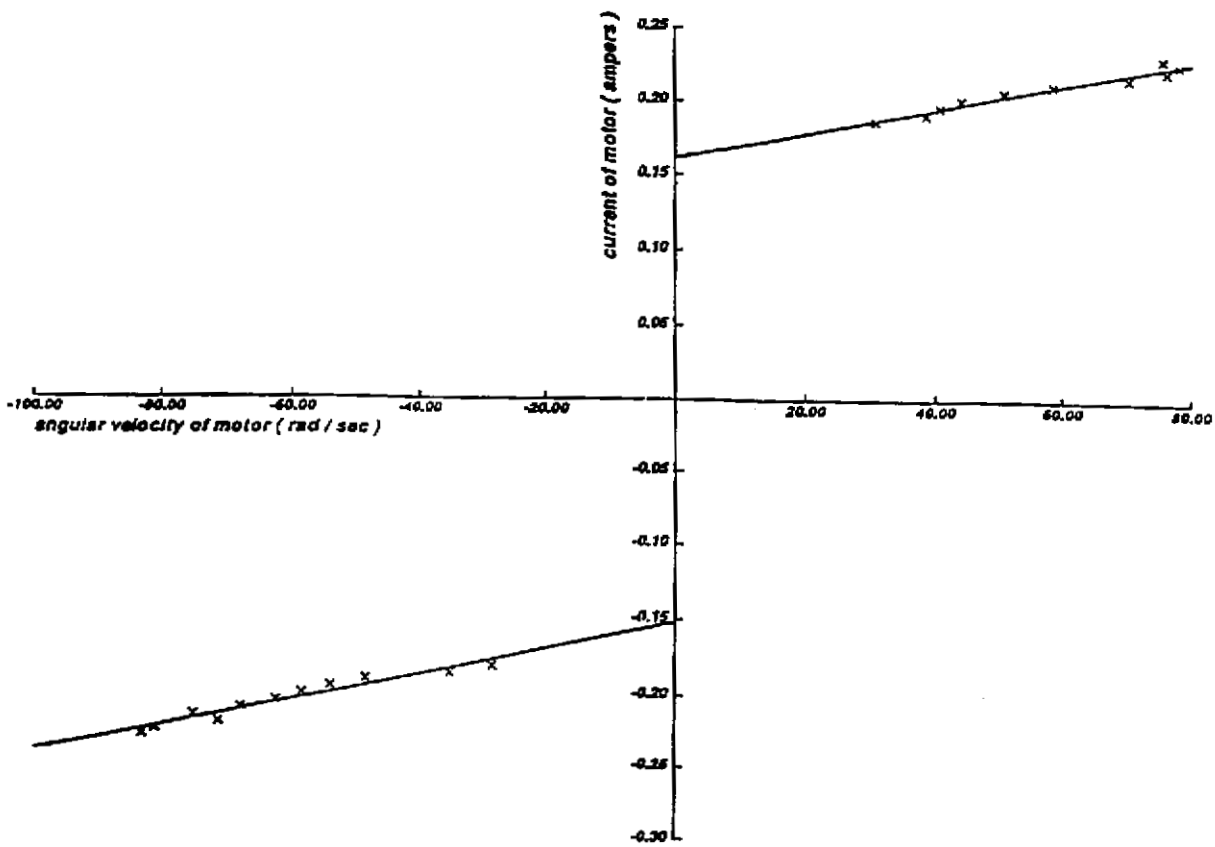

Figure 8: Characterization of friction using temporal data.

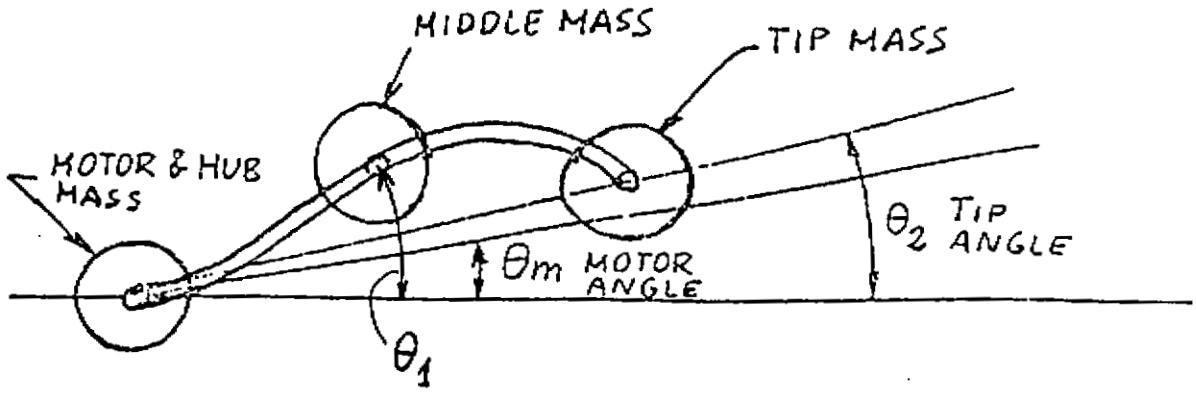

Figure 9: System nomenclature for the two-mass arm.

References

[1] Cannon, R. H., and Schmitz, E.
Precise Control of Flexible Manipulators.
Robotics Research, 1985.

[2] Matsuno, F., Fukushima, S. et al.
Feedback Control of a Flexible Manipulator with a Parallel Drive Mechanism.
International Journal of Robotics Research. Vol. 6, No. 4, Winter, 1987.

[3] Harahima, F. and Ueshiba, T.
Adaptive Control of Flexible Arm using the End-Point Position Sensing.
Proceedings Japan-Usa Symposium of Flexible Automation. Osaka (Japan), July, 1986.

[4] Siciliano, B., Yuan, B.S. and Book, W.J.
Model Reference Adaptive Control of a One Link Flexible Arm.
25th IEEE Conference on Decision and Control. Athens (Greece), December, 1986.

[5] Rovner, D.M. and Cannon, R.H.
Experiments Towards on-line Identification and Control of a Very Flexible One-Link Manipulator.
International Journal of Robotics Research. Vol. 6, No. 4, Winter, 1987.

[6] Ower, J. C. and Van de Vegte, J.
Classical Control Design for a Flexible Manipulator: Modeling and Control System Design.
IEEE Journal of Robotics and Automation. Vol. RA-3, No. 5, October, 1987.

[7] Book, W.J.
Analysis of Massless Elastic Chains with Servo Controlled Joints.
ASME Journal of Dynamic Systems, Measurements, and Control. Vol. 101. September, 1979.

[8] Truckenbrodt, A.
Dynamics and Control Methods for Moving Flexible Structures and Their Application to Industrial Robots.
Proc. of the 5th World Congress on Theory of Machines and Mechanisms. Montreal (Canada), 1979.

[9] Low, K. H.
A Systematic Formulation of Dynamic Equations for Robot Manipulators with Elastic Links.
Journal of Robotic Systems. Vol. 4(3), 1987.

[10] Feliu, V., Rattan, K.S., and Brown, H.B.
Model Identification of a Single-Link Flexible Manipulator in the Presence of Friction.
19th ISA Annual Modelling and Simulation Conference. Pittsburgh (USA), May, 1988.

[11] Rattan, K.S., Feliu, V., and Brown, H.B.
A Robust Control Scheme for Flexible Arms with Friction in the Joints.
1988 NASA - Air Force Workshop on Space, Operation, Automation and Robotics. Dayton (USA), July, 1988.

[12] Kuo, B.C.
Automatic Control Systems. Prentice-Hall, 1982.

[13] Lancaster, P., and Tismenetsky, M.
The Theory of Matrices. Second Edition with Applications. Academic Press, 1985.

[14] Hastings, G.G., and Book, W.J.
Verification of a Linear Dynamic Model for Flexible Robotic Manipulators.
Proceedings, 1986 International Conference on Robotics and Automation. San Francisco (USA), April, 1986.

[15] Canudas, C., Astrom K.J., and Braun K.
Adaptive Friction Compensation in DC-Motor Drives.
IEEE Journal of Robotics and Automation. Vol. RA-3, n-6, December, 1987.

[16] Oppenheim, A. V., and Schafer, R. W.
Digital Signal Processing. Prentice-Hall, 1975.